Atmos. Chem. Phys., 16, 13807–13821, 2016
www.atmos-chem-phys.net/16/13807/2016/
doi:10.5194/acp-16-13807-2016

Atmospheric Chemistry and Physics
Open Access
EGU

Speciated atmospheric mercury on haze and non-haze days in an inland city in China

Qianqian Hong[1,3], Zhouqing Xie[1,2,3], Cheng Liu[1,2,3], Feiyue Wang[4], Pinhua Xie[2,3], Hui Kang[1], Jin Xu[2], Jiancheng Wang[1], Fengcheng Wu[2], Pengzhen He[1], Fusheng Mou[2], Shidong Fan[1], Yunsheng Dong[2], Haicong Zhan[1], Xiawei Yu[1], Xiyuan Chi[1], and Jianguo Liu[2]

[1]School of Earth and Space Sciences, University of Science and Technology of China, 230026 Hefei, China
[2]CAS Center for Excellence in Regional Atmospheric Environment& Institute of Urban Environment of CAS, 361021 Xiamen, China
[3]Key Lab of Environmental Optics and Technology, Anhui Institute of Optics and Fine Mechanics, Chinese Academy of Sciences, 230031 Hefei, China
[4]Centre for Earth Observation Science, and Department of Environment and Geography, University of Manitoba, Winnipeg, MB R3T 2N2, Canada

Correspondence to: Zhouqing Xie (zqxie@ustc.edu.cn) and Cheng Liu (chliu81@ustc.edu.cn)

Received: 1 June 2016 – Published in Atmos. Chem. Phys. Discuss.: 11 July 2016
Revised: 20 October 2016 – Accepted: 24 October 2016 – Published: 8 November 2016

Abstract. Long-term continuous measurements of speciated atmospheric mercury were conducted from July 2013 to June 2014 in Hefei, a midlatitude inland city in eastern central China that experiences frequent haze pollution. The mean concentrations (±standard deviation) of gaseous elemental mercury (GEM), gaseous oxidized mercury (GOM) and particle-bound mercury (PBM) were 3.95 ± 1.93 ng m^{-3}, 2.49 ± 2.41 and 23.3 ± 90.8 pg m^{-3}, respectively, on non-haze days, and 4.74 ± 1.62 ng m^{-3}, 4.32 ± 8.36 and 60.2 ± 131.4 pg m^{-3}, respectively, on haze days. Potential source contribution function (PSCF) analysis suggested that atmospheric mercury pollution on haze days was caused primarily by local emissions, instead of via long-range transport. The poorer mixing conditions on haze days also favored the accumulation of atmospheric mercury. Compared to GEM and GOM, PBM was especially sensitive to haze pollution. The mean PBM concentration on haze days was 2.5 times that on non-haze days due to elevated concentrations of particulate matter. PBM also showed a clear seasonal trend; its concentration was the highest in fall and winter, decreased rapidly in spring and was the lowest in summer, following the same order in the frequency of haze days in different seasons. On both non-haze and haze days, GOM concentrations remained low at night, but increased rapidly just before sunrise, which could be due to diurnal variation in air exchange between the boundary layer and free troposphere. However, non-haze and haze days showed different trends in daytime GEM and GOM concentrations. On non-haze days, GEM and GOM declined synchronously through the afternoon, probably due to the retreat of the free tropospheric air as the height of the atmospheric boundary layer increases. In contrast, on haze days, GOM and GEM showed opposite trends with the highest GOM and lowest GEM observed in the afternoon, suggesting the occurrence of photochemical oxidation. This is supported by simple box-model calculations, which showed that oxidation of GEM to GOM does occur and that the transport of free tropospheric GOM alone is not large enough to account for the observed increase in daytime GOM. Our results further postulate that NO_2 aggregation with the HgOH intermediate may be a potential mechanism for the enhanced production of GOM during daytime.

1 Introduction

Mercury (Hg) is an environmental pollutant that has received much global attention because of its toxicity and bioaccumulation in the aquatic ecosystems. The most important transport pathway of mercury is via the atmo-

sphere (Schroeder and Munthe, 1998; Lindqvist and Rodhe, 1985). Operationally, atmospheric mercury is commonly differentiated into three forms: gaseous elemental mercury (GEM), gaseous oxidized mercury (GOM) and particle-bound mercury (PBM). The sum of these three types of atmospheric speciated mercury is defined as total atmospheric mercury (TAM = GEM + GOM + PBM), and the sum of GEM and GOM is known as total gaseous mercury (TGM = GEM + GOM) (Gustin and Jaffe, 2010; Gustin et al., 2015). Globally, GEM is the dominant form of atmospheric mercury, accounting for over 95 % of the total. GEM is stable in the troposphere with a long residence time (0.5–2 years) and can be transported at the regional to global scale (Schroeder and Munthe, 1998; Lindberg et al., 2007). GEM can be photochemically oxidized to GOM, which can be converted to PBM upon adsorption on aerosol surfaces. Different from GEM, GOM and PBM can be readily removed form the air by wet and dry deposition as a result of their high surface affinity and water solubility (Lindqvist and Rodhe, 1985). Thus, chemical transformation between GEM, GOM and PBM will directly influence the atmospheric lifetime of mercury.

As a result of rapid industrial development and economic growth in recent decades, China has become one of the major contributors to anthropogenic mercury emissions to the environment (Wu et al., 2006; Pacyna et al., 2006, 2010; L. Zhang et al., 2015). Atmospheric mercury emissions from anthropogenic sources in China have been estimated to be in the range of 500–700 t year^{-1}, accounting for 25–30 % of the total global anthropogenic mercury emissions (Streets et al., 2005; Wu et al., 2006). Studies of atmospheric mercury in China are therefore critical to the understanding of mercury cycling at both regional and global scales. Long-term observation of atmospheric mercury has been conducted in numerous urban and remote areas in China. TGM concentrations in urban and industrial areas were observed to be in the range of 2.7–35 ng m^{-3}, higher than the values reported for North America and Europe, and for the nearby Asian countries such as Korea and Japan (Weigelt et al., 2013; Fang et al., 2009; Marumoto et al., 2015). TGM and PBM concentrations in remote areas of China were also found to be higher than those observed in North America and Europe (Fu et al., 2008a, b, 2012; Liu et al., 2010).

In recent years, haze pollution has become a major concern in China due to its impacts on visibility, air quality and climate. It is well known that haze formation is mainly dependent on the atmospheric relative humidity (RH) and the concentration of airborne particles (Chen et al., 2003; Sun et al., 2013). Most studies on haze have focused on the measurements of airborne particulate matter; few have examined the influence of haze on the chemistry of atmospheric mercury, especially PBM. Here we report a 1-year real-time measurement of speciated atmospheric mercury in Hefei, an inland city of China, which experiences frequent haze events. The comparison of atmospheric mercury on haze days and non-haze days allows us to examine the formation and deposition mechanisms of mercury, as well as their temporal variations.

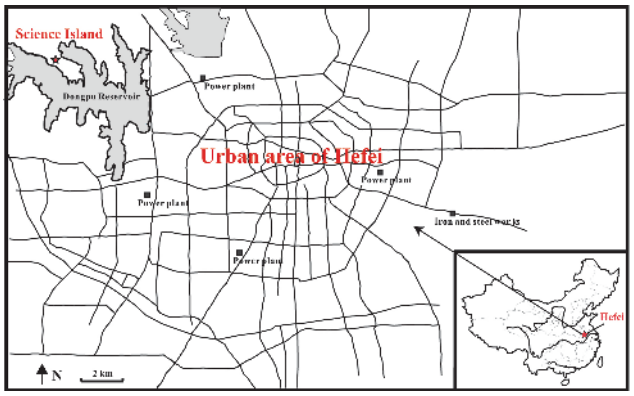

Figure 1. Location of the study site in Hefei, China.

2 Methods

2.1 Study site

Hefei (31°52′ N, 117°17′ E) is the capital of Anhui province in eastern central China, between the Changjiang (Yangtze River) and the Huaihe (Huai River). The region has a humid subtropical climate with four distinct seasons: summer (June–August), fall (September–November), winter (December–February) and spring (March–May). The prevailing wind is southeasterly in summer and northwesterly in winter. Like many Chinese cities, Hefei has experienced rapid growth in the past 20 years, with a present-day total permanent population of about 7.7 million. The city has also been witnessing an increasing frequency in haze pollution, especially in winter months.

The monitoring site was located on Science Island, a small peninsula on the Dongpu Reservoir in the northwestern outskirts of Hefei (Fig. 1). The sampling and analytical instruments were installed 1.5 m above the rooftop (∼ 20 m above the ground) of the main building of the Anhui Institute of Optics and Fine Mechanics. Further information about the monitoring site can be found in a previous study (Hu et al., 2014). We chose this area as the monitoring site because it is not near to any direct pollution sources such as power plants or iron and steel works.

2.2 Measurements of speciated atmospheric mercury

From July 2013 to June 2014, simultaneous measurements of GEM, GOM and PBM were carried out by an automated Tekran™ mercury speciation system. The system consisted of a Model 2537B mercury analyzer combined with a Model 1130 GOM unit and a Model 1135 PBM unit. The system was configured to measure GEM every 5 min, and GOM and PBM every 2 h.

The details about the Tekran™-based mercury speciation system can be found in Landis et al. (2002). In general, the automated measurement process can be summarized as sample collection, thermal desorption and determination. During the collection period, ambient air is drawn to the system at a typical flow rate of 10 L min^{-1}. GOM and PBM in the air are captured by a KCl-coated quartz annular denuder in the 1130 unit and a quartz filter in the 1135 unit, respectively, whereas GEM passes through the denuder and filter and is quantified on the 2537B analyzer by cold vapor atomic fluorescence spectroscopy (CVAFS). After 1 h of sampling, the 1135 quartz filter and the 1130 denuder are switched to the thermal decomposition mode at 800 and 500 °C, respectively, with the resulting Hg^0 quantified by the 2537B unit in the next hour, while the 1135 and 1130 components are flushed with zero-mercury gas for the next sampling.

The instrument maintenance followed typical protocols used in similar studies (Landis et al., 2002; Hu et al., 2014). The quartz annular denuder was recoated every 2 weeks, the quartz filter was replaced once a month and the Teflon filter (pore size 0.2 µm) in the sample inlet was changed every 2 weeks. Automated recalibration of the Tekran™ 2537B was performed every 25 h using an internal mercury permeation source. No calibration standards were available for GOM and PBM, but the 1σ precision for GOM and PBM was about 15 % (Landis et al., 2002). The detection limit in ambient air is about 0.5 ng m^{-3} for GEM (or TGM) at a resolution of 5 min, and 1 pg m^{-3} for GOM and PBM at a resolution of 2 h (Gustin et al., 2015). Although the Tekran™-based mercury speciation technique has been widely used around the world, recent studies have shown that the technique does not efficiently collect all GOM, and thus may substantially underestimate the concentration of reactive mercury (Huang et al., 2013; Gustin et al., 2013). Therefore, the GOM values reported in this study should be considered as the lower limit of GOM in the air (Wang et al., 2014).

2.3 Ancillary data

Standard meteorological measurements including air temperature, pressure, RH, wind direction and speed were observed with a 5 min resolution. CO was measured by an automated infrared carbon monoxide analyzer (Model EC9830T, Ecotech Inc., Australia), with a detection limit of 40 ppbv. O_3 was measured every 5 min by an ozone analyzer (Model EC9810B, Ecotech Inc., Australia); its detection limit and accuracy were 0.5 and 1 ppbv, respectively. NO_2 was measured by a multi-axis differential optical absorption spectroscopy (MAX-DOAS) instrument. The collected spectra were analyzed using the QDOAS spectral fitting software suite developed at BIRA-IASB (http://uv-vis.aeronomie.be/software/QDOAS/). $PM_{2.5}$ (particulate matter of less than 2.5 µm in diameter) data were collected from the China air quality online analysis platform (http://www.aqistudy.cn/historydata/index.php).

2.4 Potential source contribution function (PSCF) analysis

To identify the possible influence of long-range transport on the distribution of atmospheric mercury in Hefei, we calculated backward trajectories of air masses using the HYSPLIT (Hybrid Single-Particle Lagrangian Integrated Trajectory) model with the Global Data Assimilation System (GDAS 1°) developed by the National Oceanic and Atmospheric Administration (NOAA) (http://www.ready.noaa.gov) (Draxler and Hess, 1998). Considering atmospheric pollutants are mainly concentrated in low altitudes during heavy pollution days, the trajectory arrival heights were set at 500 m to represent the boundary layer where atmospheric pollutants were well mixed. In this study, 3-day back-trajectories were generated hourly by the TrajStat software, which employs HYSPLIT for trajectory calculation (Wang et al., 2009).

The contributions of other source regions to the atmospheric mercury in Hefei were identified by the potential source contribution function (PSCF) analysis with TrajStat. PSCF analysis has been shown to be useful in spatially identifying emission sources for pollutants with a long lifetime such as elemental mercury and CO (Xu and Akhtar, 2010). The study domain is divided into grid cells, and the PSCF value for each cell was calculated by counting the trajectory segment endpoints that terminate within the cell. The PSCF value for the ijth cell is defined as

$$\mathrm{PSCF}_{ij} = \frac{M_{ij}}{N_{ij}} W_{ij}, \tag{1}$$

where N_{ij} is the number of endpoints that fall in the ijth cell, and M_{ij} is the number of endpoints in the same cell that has a GEM concentration higher than an arbitrarily set criterion; in this study the criterion was set to be 4 ng m^{-3}, which is the mean GEM concentration during the entire study period. W_{ij} is an arbitrary weight function introduced to reduce the effect of small values of N_{ij} to better reflect the uncertainty in the values for these cells (Polissar et al., 2001). The weight function reduces the PSCF values when the total number of endpoints in a particular cell is less than 3 times the average value of the end points per cell:

$$W_{ij} = \begin{cases} 1.0 & N_{ij} \geq 3N_{\mathrm{ave}} \\ 0.70 & 3N_{\mathrm{ave}} > N_{ij} \geq 1.5N_{\mathrm{ave}} \\ 0.40 & 1.5N_{\mathrm{ave}} > N_{ij} \geq N_{\mathrm{ave}} \\ 0.20 & N_{\mathrm{ave}} > N_{ij} \end{cases}. \tag{2}$$

3 Results

We intended to continuously monitor speciated atmospheric mercury concentrations over the course of 1 year; however, interruptions were inevitable due to instrument maintenance, which resulted in loss of data for the following four periods: (1) 25 September to 9 October 2013; (2) 5–14 November 2013; (3) 9–25 February 2014; and (4) 1–14 April 2014.

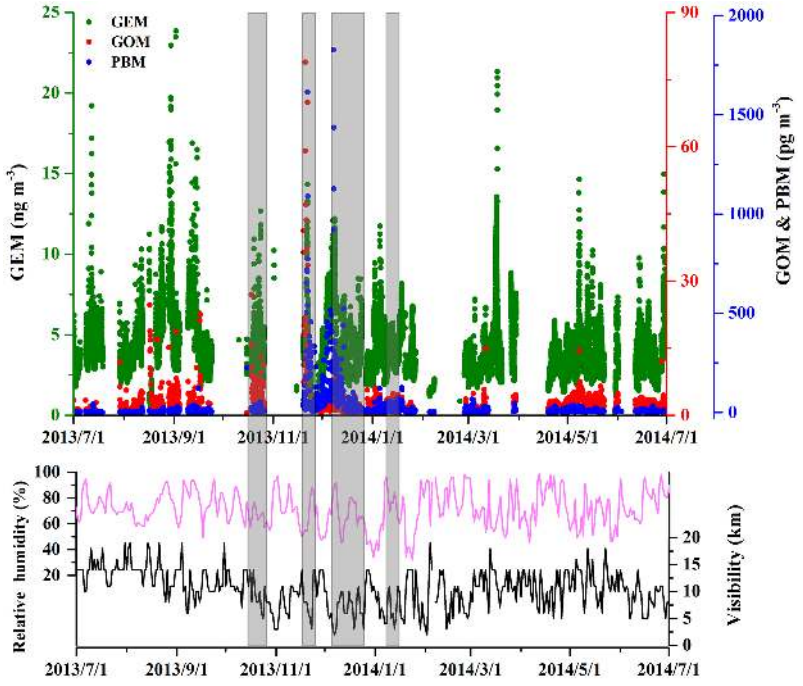

Figure 2. Time series of GEM, GOM and PBM concentrations, along with visibility and relatively humidity, at the monitoring site in Hefei from July 2013 to June 2014. The GEM data were at a 5 min resolution, and the GOM and PBM data were 2 h averages. The gray columns show the major haze pollution episodes that occurred during the study period.

The rest of the data were grouped into haze days and non-haze days according to the China Meteorological Administration's haze standard (QX/T 113-2010). Haze days refer to the days when the atmospheric visibility was < 10 km and the RH was < 80 % (Duan et al., 2016), and non-haze days refer to clear days with an atmospheric visibility > 10 km. The visibility and RH information was collected from the weather history data at the Luogang Airport of Hefei (http://www.wunderground.com/). Throughout the study period of almost 1 year, a total of 56 days were identified to be haze days, and 253 days to be non-haze days. All the times reported herein are local time (UTC + 8 h).

3.1 Overall characteristics of speciated atmospheric mercury

The time series of GEM, GOM and PBM concentrations at the study site throughout the study period are shown in Fig. 2; their frequency distributions are shown in Fig. S1 in the Supplement. The mean (±standard deviation) GEM, GOM and PBM concentrations during the entire study period were 4.07 ± 1.91 ng m^{-3}, 3.67 ± 5.11 and 30.0 ± 100.3 pg m^{-3}, respectively (Table 1). GEM concentrations in different seasons did not differ much, with the highest in fall (4.51 ± 2.10 ng m^{-3}) and the lowest in spring (3.89 ± 1.79 ng m^{-3}). GOM concentrations varied greatly, with much higher concentrations in fall and the lowest in winter. A similar seasonal variation in the GOM concentration was observed at a remote site in Mt. Gongga of southwestern China (Fu et al., 2008b). PBM showed the highest degree of seasonal variability; its concentration decreased in the following order: fall ≈ winter > spring > summer. The mean PBM concentrations in fall and winter were about 20 times that in summer, similar to the findings from many previous studies in China (Zhang et al., 2013; Fu et al., 2011, 2008b; Fang et al., 2001).

Comparisons of speciated atmospheric mercury concentrations with other urban and rural areas in China and a few other countries are shown in Table 2. The mean GEM concentration in Hefei is slightly higher than the concentrations reported from many remote areas in China (Fu et al., 2008a, b, 2012; Wan et al., 2009a, b; H. Zhang et al., 2015), but is much lower than the concentrations from urban areas of heavily industrial cities such as Guiyang and Changchun, where large point sources of mercury exist (e.g., nonferrous metal smelting, coal-fired power plants and residential coal burning) (Feng et al., 2004; Fu et al., 2011; Fang et al., 2004). Although Hefei is geographically close to Shanghai, a mega urban center in China, it is interesting to note that the TGM concentration of Shanghai is much lower than that of Hefei. This may be due to the fact that Shanghai is a coastal city that is influenced more by cleaner marine air masses (Friedli et al., 2011). Table 2 also shows that the average concentration of GEM in Hefei is double the typical values reported from the urban and rural areas in Europe and North America (Liu et al., 2010; Li et al., 2008; Brooks et al., 2010).

Table 1. Summary of GEM, GOM and PBM concentrations measured in Hefei from July 2013 to June 2014.

	GEM (ng m^{-3})			GOM (pg m^{-3})			PBM (pg m^{-3})		
	Mean $\pm\sigma$	Range	N	Mean $\pm\sigma$	Range	N	Mean $\pm\sigma$	Range	N
Spring	3.89 ± 1.79	0.2–21.3	7890	4.49 ± 4.22	0.5–69.8	526	8.34 ± 8.97	1.6–130.1	542
Summer	4.08 ± 1.99	0.3–22.9	6050	3.66 ± 4.39	0.5–45.2	511	3.61 ± 4.38	0.5–41.9	570
Fall	4.51 ± 2.10	0.4–23.8	3632	5.65 ± 8.93	0.5–78.9	274	59.9 ± 153.5	0.5–1615	339
Winter	4.05 ± 1.81	0.9–12.2	6381	2.59 ± 2.58	0.5–9.5	541	56.1 ± 134.9	0.5–1827	639
Total	4.07 ± 1.91	0.2–23.8	23 953	3.67 ± 5.11	0.5–78.9	1852	30.02 ± 100.3	0.5–1827	2090
Non-haze	3.95 ± 1.93	0.2–23.8	20 345	2.49 ± 2.41	0.5–33.5	1508	23.3 ± 90.76	0.5–1827	1708
Haze	4.74 ± 1.62	2.1–16.5	3608	4.32 ± 8.36	0.5–78.9	344	60.2 ± 131.4	1.6–1615	382

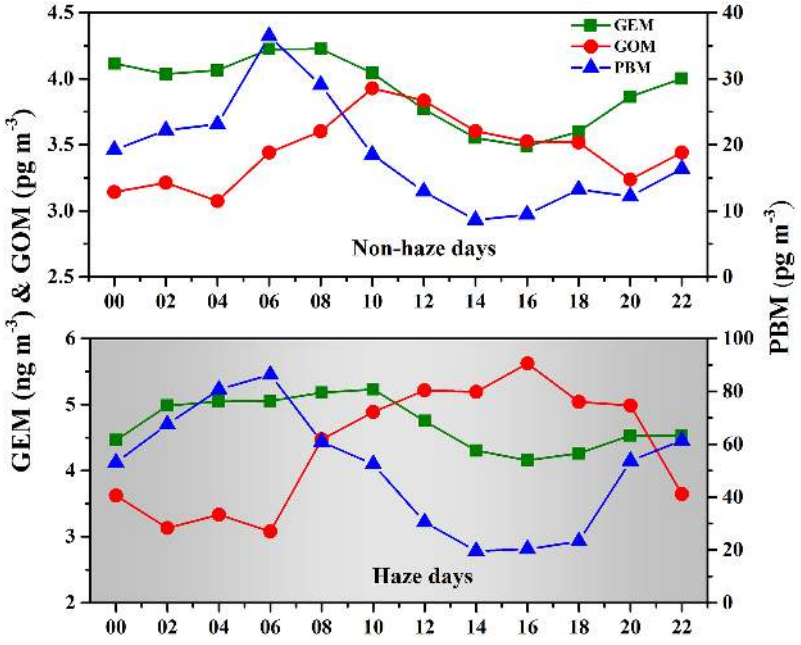

Figure 3. Diurnal trends of GEM, GOM and PBM concentrations in Hefei on non-haze and haze days (local time = UTC + 8 h). The data were 2 h averages.

3.2 Speciated atmospheric mercury on non-haze days

As shown in Table 1 and Fig. S1 (in blue), the mean concentration of GEM on non-haze days was 3.95 ± 1.93 ng m^{-3}. Its distribution was characterized by large variations ranging from 0.2 to 23.8 ng m^{-3}, although more than half of the GEM values were in the narrow range 2–4 ng m^{-3}. The mean concentration of GOM on non-haze days was 2.49 ± 2.41 pg m^{-3}, with a range of 0.5–33.5 pg m^{-3}, although most of the values were in the range of 1–4 pg m^{-3}. High concentrations of GOM (exceeding 10 pg m^{-3}) only accounted for 1.4 % of the total data points. The mean GOM concentration in Hefei on these non-haze days is much smaller than the concentrations reported from other study sites in China (Table 2), but is comparable to the values observed at many European and North American sites (Peterson et al., 2012; Cheng et al., 2014; Ren et al., 2016). The mean PBM concentration on non-haze days was 23.3 ± 90.8 pg m^{-3}, with an exceptionally large range of 0.5–1827 pg m^{-3}; high PBM concentrations (i.e., > 50 pg m^{-3}) accounted for 6.4 % of the total data points. The PBM concentration under non-haze conditions in Hefei is generally similar to values reported from remote areas in western China, such as Mt. Gongga, Mt. Waliguan and Shangri-La.

Diurnal variations of GEM, PBM and GOM concentrations on non-haze days are shown in Fig. 3. Both GEM and PBM concentrations exhibited similar patterns, with elevated concentrations at night. The GOM concentration remained relatively constant at night, but increased rapidly just before sunrise and reached its peak value at $\sim$ 10:00 UTC + 8 h, followed by a synchronous decline with GEM through the afternoon (10:00–18:00).

Table 2. Speciated atmospheric mercury concentrations in Hefei and other urban and rural areas.

Location	Classification	Time	TGM ($ng\,m^{-3}$)	GEM ($ng\,m^{-3}$)	GOM ($pg\,m^{-3}$)	PBM ($pg\,m^{-3}$)	Reference
Hefei	Suburb	Jul 2013–Jun 2014	4.1	4.07	3.67	30	This study
Hefei	Suburb	Feb–May 2009	2.53	–	–	–	Hu et al. (2014)
Beijing	Rural	Dec 2008–Nov 2009	3.23	3.22	10.1	98.2	Zhang et al. (2013)
Shanghai	Urban	Aug–Sep 2009	2.7	–	–	–	Friedli et al. (2011)
Nanjing	Urban	Jan–Dec 2011	7.9	–	–	–	Zhu et al. (2012)
Guiyang	Urban	Nov 2001–Nov 2002	8.4	–	–	–	Feng et al. (2004)
Guiyang	Urban	Aug–Dec 2009	–	9.72	35.7	368	Fu et al. (2011)
Changchun	Urban	Jul 1999–Jan 2000	18.4	–	–	276	Fang et al. (2004)
Changchun	Suburb	Jul 1999–Jan 2000	11.7	–	–	109	Fang et al. (2004)
Mt. Changbai	Remote	Aug 2005–Jul 2006	3.58	–	65	77	Wan et al. (2009a, b)
Mt. Gongga	Remote	May 2005–July 2006	3.98	–	6.2	30.7	Fu et al. (2008a, b)
Mt. Waliguan	Remote	Sep 2007–Aug 2008	1.98	–	7.4	19.4	Fu et al. (2012)
Mt. Leigong	Remote	May 2008–May 2009	2.8	–	–	–	Fu et al. (2010)
Shangri-La	Remote	Nov 2009–Nov 2010	2.55	–	8.22	38.82	L. Zhang et al. (2015)
Detroit, USA	Urban	Jan–Dec 2004	–	2.5	15.5	18.1	Liu et al. (2010)
Dexter, USA	Rural	Jan–Dec 2004	–	1.6	3.8	6.1	Liu et al. (2010)
Houston, USA	Urban	Aug–Oct 2006	–	1.66	6.9	2.5	Brooks et al. (2010)
Florida, USA	Urban	Jul 2009–Jul 2010		1.3	3	2	Peterson et al. (2012)
Maryland, USA	Suburb	2007–2015		1.41	4.6	8.6	Ren et al. (2016)
Gothenburg, Sweden	Urban	Feb–Mar 2005	–	1.96	2.53	12.5	Li et al. (2008)
Nova Scotia, Canada	Urban	Jan 2010– Dec 2011		1.67	2.07	2.32	Cheng et al. (2014)
Northern Hemisphere background value				1.5–1.7			Lindberg et al. (2007)

3.3 Speciated atmospheric mercury on haze days

Haze pollution mainly occurred in December and January at our monitoring site. The four major haze pollution periods were identified in gray in Fig. 2. The mean concentrations of GEM, GOM and PBM on these haze days were $4.74 \pm 1.62\,ng\,m^{-3}$, 4.32 ± 8.36 and $60.2 \pm 131.4\,pg\,m^{-3}$, respectively (Table 1). The frequency distributions of GEM, GOM and PBM on the haze days are shown in Fig. S1 (in gray). GEM, GOM and PBM concentrations show significant differences between haze and non-haze days ($p < 0.001$, t test) (Fig. S2). On average, the concentration of GEM on haze days was 1.2 times that on non-haze days. Similarly, the concentration of GOM on haze days was about 1–1.7 times that on non-haze days. The largest impact of haze pollution is, however, on PBM, with the mean PBM concentration on haze days about 2.5 times that on non-haze days. High concentrations of GOM (exceeding $10\,pg\,m^{-3}$) and PBM concentrations (exceeding $50\,pg\,m^{-3}$) were also more frequently observed on haze days, accounting for 5.9 and 25 %, respectively, of the total haze days.

As shown in Fig. 3, on haze days the GEM concentration was higher at night and lower during daytime. PBM typically peaked just before sunrise, with the lowest values occurring in the afternoon (14:00–16:00). The opposite pattern was observed for GOM, which showed higher concentrations during daytime than at night. Although on both haze and non-haze days GOM showed rapid increase just before sunrise, they exhibited different trends during daytime from 10:00 to 18:00. On haze days, GOM peaked in the afternoon when GEM was the lowest; the duration of the afternoon GOM peak was also longer on haze days.

4 Discussion

4.1 Influence of atmospheric mercury emission source

With the year-long data seasonal mercury emission sources could be inferred from the PSCF analysis. Figure 4a showed the overall spatial contribution of mercury emission sources in China. As Hefei is located in eastern central China, its atmospheric mercury concentration could be affected by both northern and southern emission sources, including those from the North China Plain (especially Shandong province) and the neighboring provinces of Henan, Jiangsu, Jiangxi and Hubei. The total mercury emissions from Henan and Shandong provinces were estimated to be over 50 and 45 t in 2010, respectively, making them two of the largest Hg emitters in China (L. Zhang et al., 2015). Long-range transport could also impact seasonal variations of atmospheric mercury in Hefei. As shown in Fig. 4, in spring, the major contributors of atmospheric mercury to Hefei were from the southwestern region, including the local area and Jiangxi and Henan provinces. In summer, the main contributors were from north of Anhui, as well as Henan and Jiangxi provinces, and even from the Pearl River Delta region in the far south. Since the number of haze days only accounts for 5.6 % of the total days in spring and summer, we did not provide haze and

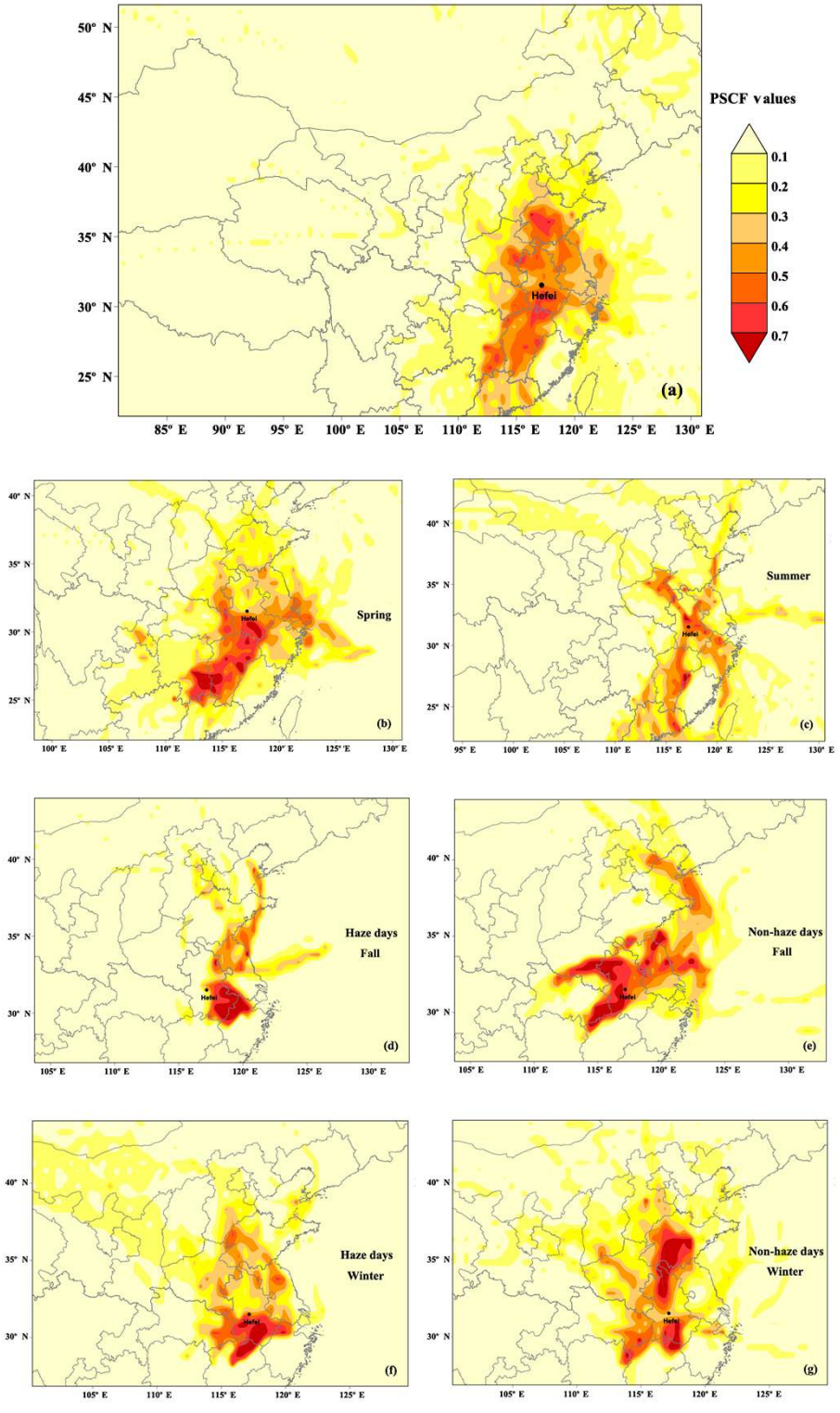

Figure 4. Likely emission source areas of GEM identified by PSCF analysis. **(a)** Overall (from July 2013 to June 2014), **(b)** spring, **(c)** summer, **(d)** haze days in fall, **(e)** non-haze days in fall, **(f)** haze days in winter, **(g)** non-haze days in winter.

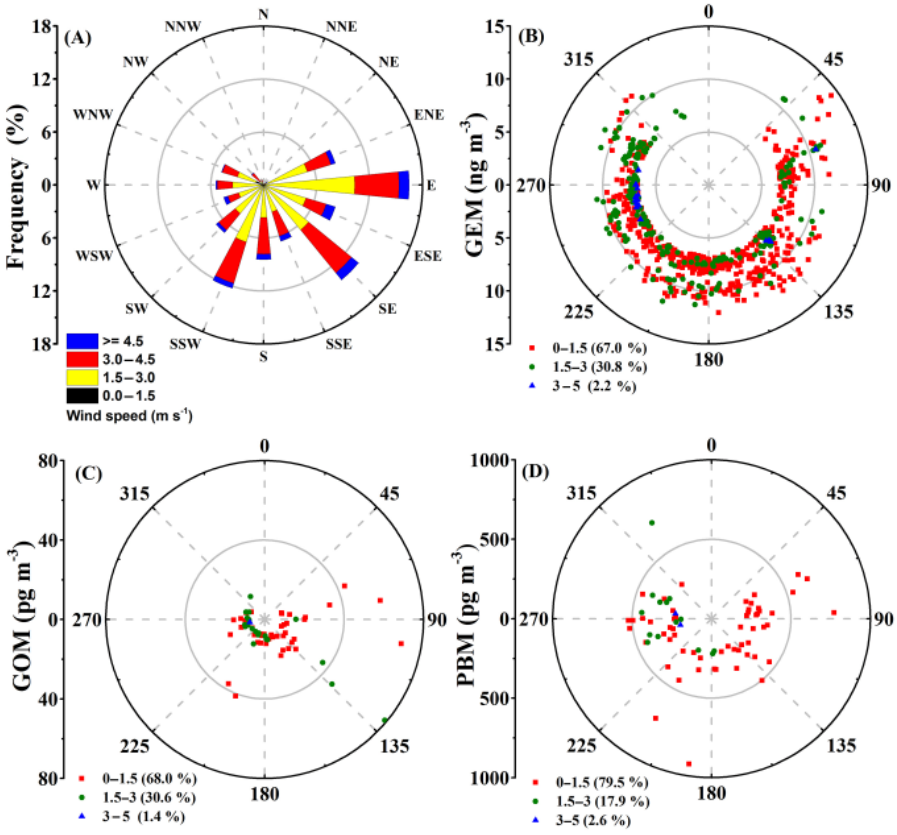

Figure 5. Wind direction and speed at the monitoring station during the study period. **(a)** The wind rose for the entire study period; **(b, c, d)** are the wind rose diagrams for GEM, GOM and PBM concentrations above the 90th percentile values, respectively.

non-haze PSCF results for spring and summer seasons. As fall and winter are the prevalent seasons for haze pollution, one PSCF result for haze days and another for non-haze days are shown for fall and winter, respectively. The statistically significant difference ($p < 0.001$) in the GEM concentration between non-haze days and haze days suggests that haze pollution could directly affect the concentration of elemental mercury. As shown in Fig. 4d and f, higher GEM concentration was mainly influenced by local emission sources on haze days. On non-haze days, the most important mercury sources to the monitoring site were not only the local emission sources, but also those from the neighboring regions of Shandong, Henan and Jiangxi provinces (see Fig. 4e and g). Therefore, the increase in the GEM concentration on haze days was mainly caused by local emissions.

GEM and CO often share similar anthropogenic emission sources, such as industrial coal combustion, domestic coal combustion, iron and steel production and cement production (Wu et al., 2006; Wang et al., 2005). However, they also have their distinct emission sources. For instance, power plants and nonferrous metal smelters emit mercury but hardly any CO; while automobiles contribute greatly to CO emission, they are not a major emitter for mercury. The correlation coefficients and slopes between GEM and CO concentrations during mercury pollution events are shown in Table 3. These mercury pollution episodes were defined as when the hourly average GEM concentration was higher than seasonal average GEM concentration for at least 10 consecutive hours. These episodes could be classified into long-range transport episodes or local episodes by using the coefficients of determination (R^2) of linear regression between Hg and CO: a significant positive correlation indicates long-range transport episodes, and a poor correlation signals local episodes (Jaffe et al., 2005; Weiss-Penzias et al., 2006; Kim et al., 2009). Using this approach, we identified three local episodes (events: 1–3) characterized by poor correlations between GEM and CO concentrations (R^2: 0.23–0.29), and four long-range transport episodes (events: 4–7) characterized by positive correlations between GEM and CO concentrations (R^2: 0.51–0.79). These local episodes tend to occur in fall and winter. The slope of the trend line represents the Hg / CO ratio, which could aid in the identification of specific emission sources. Emissions from power plants typically have a higher Hg / CO ratio (Wu et al., 2006), whereas residential coal and biomass burning combustion have a lower Hg / CO ratio (0.0013–0.0046 ng m^{-3} $ppbv^{-1}$) due to incomplete combustion (Weiss-Penzias et al., 2007). The Hg / CO ratio for vehicles is close to zero (Zhang et al.,

Table 3. Coefficients of determination and slopes between GEM and CO concentrations during atmospheric mercury pollution episodes (* $p < 0.01$).

Event	Start time (yyyy/mm/dd, UTC + 8 h)	End time (yyyy/mm/dd, UTC + 8 h)	Duration (h)	GEM (ng m^{-3})	CO (ppbv)	GEM/CO (slope, ng m^{-3} ppbv^{-1})	R^2
1	2013/11/21 03:00	2013/11/22 02:00	23	8.37 ± 2.42	4481.6 ± 717.3	0.0018	0.29*
2	2013/12/07 04:00	2013/12/09 04:00	48	9.21 ± 1.16	5943.8 ± 1394.1	0.0004	0.23*
3	2014/01/17 22:00	2014/01/19 13:00	39	5.80 ± 0.83	5746.3 ± 1626.9	0.0003	0.28*
4	2014/01/25 02:00	2014/01/25 22:00	20	6.03 ± 0.50	8797.9 ± 2244.3	0.0002	0.59*
5	2014/03/16 05:00	2014/03/16 20:00	15	4.46 ± 0.47	2261.7 ± 440.2	0.0010	0.79*
6	2014/03/17 06:00	2014/03/18 12:00	30	8.85 ± 2.46	2697.1 ± 590.3	0.0030	0.51*
7	2014/05/21 00:00	2014/05/21 11:00	11	5.74 ± 0.94	3676.7 ± 1690.0	0.0050	0.79*

Notes: these episodes were identified when the hourly average GEM concentration was higher than the seasonal average GEM concentration for more than 10 consecutive hours.

2013). The Hg / CO ratios during the pollution episodes in our study ranged from 0.0001 to 0.005 ng m^{-3} ppbv^{-1}, suggesting that mercury emission in fall and winter in Hefei could be related to local incomplete combustion sources, such as residential coal and biomass burning.

4.2 Impacts of meteorological factors for atmospheric mercury on haze days

Meteorological conditions, especially wind direction and speed, could also impact atmospheric mercury on haze days. The wind rose for the monitoring site during the study period is shown in Fig. 5. Easterly and southeasterly winds represented the prevailing wind directions at the study site. A wind rose diagram of GEM concentrations above the 90th percentile value is shown in Fig. 5b. We found that 67 % of the high GEM concentrations occurred at low wind speed (below 1.5 m s^{-1}); however, wind speed below 1.5 m s^{-1} accounted for only 1.7 % of the study duration. High GOM and PBM concentrations appear not to be related to high wind speed (wind speed: 3–5 m s^{-1}); only 1.4 and 2.6 % of the high GOM and PBM concentrations were observed under high wind speed conditions, respectively (Fig. 5c and d). The occurrence of high atmospheric mercury levels under low wind speed conditions is to be expected, as this slow wind speed condition is not conducive to the spread and mixing of mercury especially on haze days, and thus favors mercury accumulation in the air. This further supports the finding that atmospheric mercury on haze days is mainly due to local emissions.

Both GEM and PBM concentrations exhibited diurnal variations with elevated concentrations at night or in early morning, regardless of the presence of haze. Such a diurnal variation could be related to changes in the height of the urban boundary layer. The diurnal trend of the boundary layer height (BLH) in Hefei is shown in Fig. S3, which is typically low in the morning and night, and high during the daytime on both non-haze and haze days. Such diurnal changes

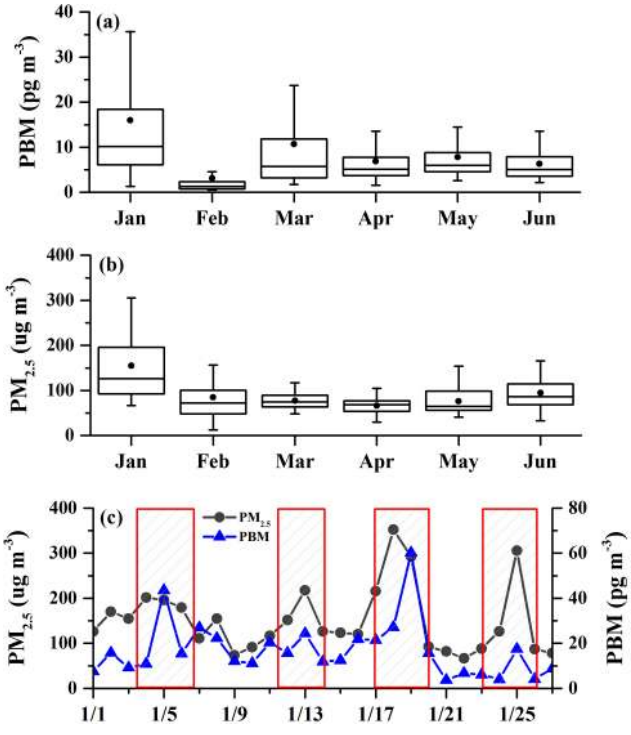

Figure 6. Monthly variation of **(a)** PBM and **(b)** $PM_{2.5}$ concentrations from January to June 2014; **(c)** average daily $PM_{2.5}$ and PBM concentrations in January 2014.

in BLH in Hefei and nearby cities have also been observed in previous studies (Yuan et al., 2005; Mao et al., 2006). The maximum PBM concentration (observed at 06:00) was more than 4 times higher than the minimum value (observed at 16:00) on both non-haze and haze days, with a 76 % decrease from early morning to the afternoon. However, the reduction of PBM as a result of deposition during haze days was 62.7 pg m^{-3}, which was about 2.4 times that on non-haze days, suggesting that haze pollution could increase the removal of PBM. Although PBM is not the major form of

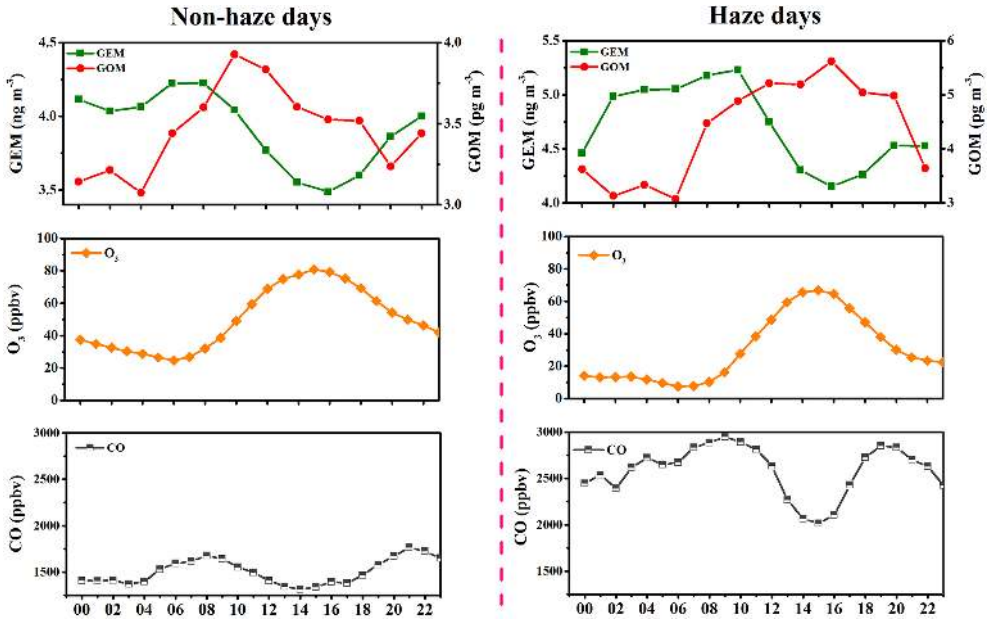

Figure 7. Diurnal variations of GEM, GOM, O_3 and CO concentrations on non-haze and haze days.

atmospheric mercury, it is crucial in atmospheric mercury transport and removal processes due to its short atmospheric lifetime. As shown in Fig. 6, the highest PBM and $PM_{2.5}$ concentrations were observed in January, which is most likely due to a shallower boundary layer in January than in other months. The co-variation in February is weaker, possibly due to the loss of PBM data because of instrument maintenance. The PBM concentration co-varied with the $PM_{2.5}$ concentration, especially in January when all the four PBM peak events were associated with increased $PM_{2.5}$ concentrations (Fig. 6c). These results suggest that $PM_{2.5}$ may play an important role in the formation of PBM. Thus, elevated PBM concentrations in fall and winter might be due to the combination of poor mixing conditions and higher PM concentrations.

4.3 Enhancement in GOM and the potential GEM oxidation mechanism

Diurnal variations of GEM, GOM, O_3 and CO concentrations on non-haze and haze days are shown in Fig. 7. The weak correlation ($r = 0.164$) between GOM and CO suggests that the CO-producing primary emission is not a major source of GOM in the air. This is clearly shown in Fig. 7 (haze days), where the peak value of GOM coincided with the lowest value of CO. As mentioned earlier, on both non-haze and haze days, GOM concentrations remained relatively constant during night, but increased rapidly prior to sunrise. However, GOM showed different trends during daytime (10:00–18:00) between non-haze and haze days. On non-haze days, a synchronous decline was found between GEM and GOM in the afternoon, but the opposite trend was observed between GEM and GOM on haze days. This difference indicates that different GOM formation mechanisms might be at work on non-haze and haze days. Two processes can affect the GOM concentrations in the boundary layer air. The first is the change in the atmospheric boundary layer height, which could change the transport of GOM-enriched free tropospheric air. Secondly, in situ photochemical oxidation of GEM would increase the GOM concentration during daytime. Various atmospheric oxidants are capable of oxidizing GEM to GOM, including halogen radicals, ozone, hydroxyl radicals (OH), among others (Holmes et al., 2010; Wang et al., 2014).

It is well established that free troposphere (FT) contains higher GOM concentrations than in the boundary layer (e.g., Murphy et al., 2006; Lyman and Jaffe, 2012; Timonen et al., 2013; Brooks et al., 2014; Shah et al., 2016). On both non-haze and haze days, it is thus possible that the higher GOM concentrations observed prior to sunrise are due to enhanced admixing of the free tropospheric air as the boundary layer increases in the morning (see Fig. S3). On non-haze days, a synchronous decline in GEM and GOM throughout afternoon (10:00–18:00) might be related to the higher atmospheric boundary layer height during this period. However, on haze days, the opposite variation was observed between GEM and GOM from 10:00 to 18:00, along with the elevated boundary layer height. This suggests that other than FT transport, photochemical oxidation of GEM might also play an important role in the enhancements of GOM. To determine the relative importance of FT transport and in situ photochemical oxidation, we examined the relationship between GOM and the changes in the height of the atmospheric

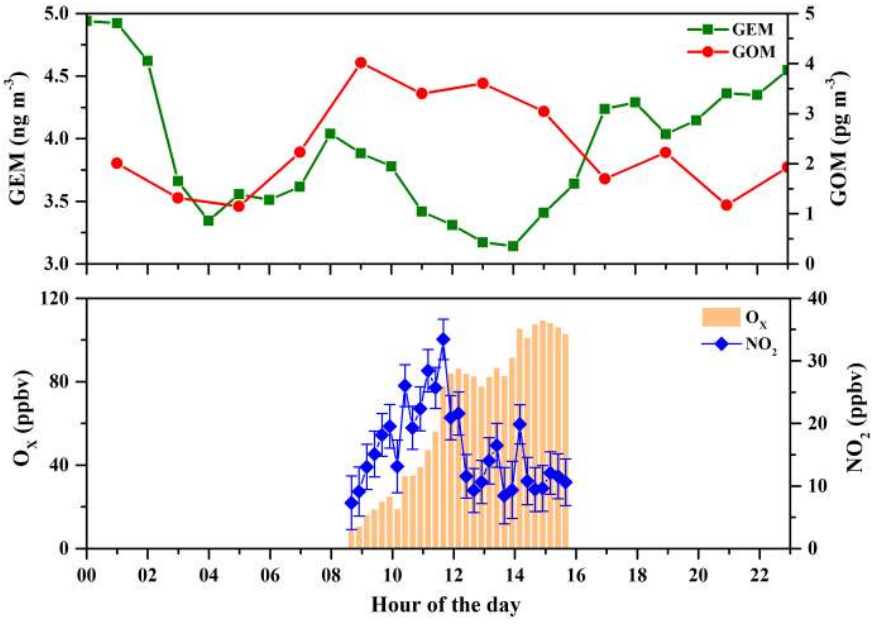

Figure 8. A case study of diurnal variations of GEM, GOM, O_x and NO_2 in Hefei (20 November 2013). The top panel shows the hourly averaged GEM and GOM concentrations, and the bottom panel shows the O_x ($O_x = NO_2 + O_3$) and the NO_2 concentrations. The error bars for NO_2 refer to the NO_2 standard errors.

Table 4. The production of NO_2HgOH and d[NO_2HgOH]/dtat different NO_2 concentrations.

NO_2 (ppbv)	10	20	30	40	50	60	70	80	90	100
$d(NO_2HgOH)/dt$ (molecule cm^{-3} s^{-1})	0.36	0.71	1.04	1.37	1.68	1.99	2.28	2.56	2.83	3.10
NO_2HgOH (pg m^{-3}, 1 h)	0.56	1.10	1.63	2.13	2.61	3.08	3.54	3.97	4.40	4.81

boundary layer and the odd oxygen ($O_x = O_3 + NO_2$) concentrations. We used O_x because it is a more conserved tracer of the extent of photochemical processes in the urban atmosphere (Herndon et al., 2008; Wood et al., 2010), as O_3 reacts with NO emitted from automobiles to form NO_2. Example results are shown in Fig. 8 for 20 November 2013 (haze day). As can be seen from the figure, GEM and GOM showed opposite trends in the afternoon (12:00–16:00), along with higher O_x concentrations during this period. The height of the atmospheric boundary layer changed very little (less than 0.1 km) over the same period (see Fig. S4). This simple comparison suggests that the transport of FT GOM might be limited and that at least some of the GOM was formed from in situ oxidation of GEM. Note that in our studies we could only calculate daytime O_x concentrations because NO_2 concentrations from MAX-DOAS were only available during daytime.

We further investigated the mechanism of GEM oxidation to GOM. Ozone itself is not an efficient oxidant for GEM oxidation due to the low reaction rate (Hall, 1995; Holmes et al., 2010). Instead, halogen radicals (especially bromine atoms) and OH radicals are believed to be the primary oxidants for GEM in the global troposphere (Holmes et al., 2010). Unfortunately, we did not measure halogen radicals in this study. OH radicals are known to be present in the early morning urban boundary layer, primarily from the photolysis of HONO, which accumulates during night (Kleffmann et al., 2005). Therefore, here we consider the oxidation of GEM by OH radicals only. The formation of HgOH as an intermediate product of the $Hg^0(g) + OH$ oxidation reactions has been proposed by Sommar et al., 2001, although HgOH is highly unstable and could decompose back rapidly to Hg^0 and OH (Sommar et al., 2001; Goodsite et al., 2004). It has been proposed that the presence of other gases X ($X = NO_2$, HO_2, RO, RO_2, or NO) could assist the formation of Hg(II) by forming X–HgOH, which outcompetes the decomposition of HgOH (Calvert and Lindberg, 2005; Dibble et al., 2012; Wang et al., 2014). As an example, we calculated the transformation between GEM and GOM under the influence of NO_2, using the reactions and rate con-

stants shown in Table S1. As shown in Fig. S5, the production rate of NO_2HgOH, $d[NO_2HgOH]/dt$, increased almost linearly with increasing NO_2 under low NO_2 concentrations, and eventually reached a steady state when the NO_2 concentration was high enough.

Based on the production rate of NO_2HgOH, we can estimate the production of NO_2HgOH during the 1 h sampling period when GOM was captured by the KCl-coated denuder in the Tekran™ 1130 unit. The production of NO_2HgOH and $d[NO_2HgOH]/dt$ corresponding to different NO_2 concentrations is shown in Table 4. With the increase of the NO_2 concentration, the contribution of the NO_2HgOH production to GOM will increase. If the NO_2 concentration is within 100 ppbv (from 0 to 100 ppbv), the production of NO_2HgOH would be in the range of 0.058–4.81 pg m^{-3} during the 1 h sampling period. As illustrated in Table 4, the level of NO_2 observed in our study is high enough to account for the increase in the observed GOM production. Our results thus support a recent study in the tropical equatorial Pacific (Wang et al., 2014) that NO_2 aggregation with HgOH provides a possible mechanism for enhanced production of GOM. If that is true, NO_2 would be expected to play an even more important role in the urban air because of its higher concentration. More laboratory and modeling studies on the mercury oxidation mechanism in the presence of NO_2 and other gases are thus warranted.

5 Summary

Continuous measurements of speciated atmospheric mercury were conducted in Hefei, a midlatitude inland city in central China, from July 2013 to June 2014. Measurements of other trace gases (e.g., CO, O_3, NO_2) and meteorological parameters were employed to better understand the sources and oxidation pathways of atmospheric mercury. The mean GEM, GOM and PBM concentrations during haze days were 4.74 ± 1.62 ng m^{-3}, 4.32 ± 8.36 and 60.2 ± 131.4 pg m^{-3}, respectively. Potential source contribution function (PSCF) analysis suggested that the local mercury emission rather than long-range transport is the most important contributor of atmospheric mercury pollution on haze days at our monitoring site. The low GEM / CO ratio in Hefei could be indicative of local incomplete combustion sources such as residential coal and biomass burning. Haze pollution has a more profound impact on PBM than on GEM and GOM. PBM showed a remarkable seasonal pattern, with higher concentrations in cold seasons and lower concentrations in warm seasons. Elevated PBM concentrations might be due to both the high loadings of particle matter and poorer mixing conditions on haze days, especially in cold months. Both GEM and PBM concentrations exhibited great variations with elevated concentration during the night. The diurnal variations of GEM and PBM might be related to the boundary layer depth; a lower boundary layer depth in the morning and night could elevate the mercury concentration.

Different from the diurnal variations of GEM and PBM, GOM concentration remained relatively constant at night, and then increased rapidly prior to sunrise. The enhancement of GOM during daytime could be due to both the transport of GOM-enriched free tropospheric air to the boundary layer and in situ oxidation of GEM in the boundary layer. Simple photochemical modeling supports the occurrence of daytime oxidation of GEM to GOM. Based on HgOH as an intermediate product, our calculations suggest that NO_2 aggregation with HgOH is a potential mechanism for the enhanced production of GOM in the inland urban air.

6 Data availability

Requests for data sets and materials should be addressed to Zhouqing Xie (zqxie@ustc.edu.cn) or Cheng Liu (chliu81@ustc.edu.cn).

The Supplement related to this article is available online at doi:10.5194/acp-16-13807-2016-supplement.

Acknowledgements. This research was supported by grants from the National Basic Research Program of China (2013CB430000), the National Natural Science Foundation of China (project nos. 91544103,41575021) and the External Cooperation Program of BIC, CAS (project no. 211134KYSB20130012).

Edited by: A. Pszenny
Reviewed by: two anonymous referees

References

Brooks, S., Luke, W., Cohen, M., Kelly, P., Lefer, B., and Rappenglück, B.: Mercury species measured atop the Moody Tower TRAMP site, Houston, Texas, Atmos. Environ., 44, 4045–4055, 2010.

Brooks, S., Ren, X., Cohen, M., Luke, W. T., Kelley, P., Artz, R., Hynes, A., Landing, W., and Martos, B.: Airborne vertical profiling of mercury speciation near Tullahoma, TN, USA, Atmosphere, 5, 557–574, 2014.

Calvert, J. G. and Lindberg, S. E.: Mechanisms of mercury removal by O_3 and OH in the atmosphere, Atmos. Environ., 39, 3355–3367, 2005.

Chen, L.-W. A., Chow, J. C., Doddridge, B. G., Dickerson, R. R., Ryan, W. F., and Mueller, P. K.: Analysis of a summertime $PM_{2.5}$ and haze episode in the mid-Atlantic region, J. Air Waste Manage., 53, 946–956, 2003.

Cheng, I., Zhang, L., Mao, H., Blanchard, P., Tordon, R., and Dalziel, J.: Seasonal and diurnal patterns of speciated atmospheric mercury at a coastal-rural and a coastal-urban site, Atmos. Environ., 82, 193–205, 2014.

Dibble, T. S., Zelie, M. J., and Mao, H.: Thermodynamics of reactions of ClHg and BrHg radicals with atmospherically abundant free radicals, Atmos. Chem. Phys., 12, 10271–10279, doi:10.5194/acp-12-10271-2012, 2012.

Draxler, R. R. and Hess, G.: An overview of the HYSPLIT_4 modelling system for trajectories, Aust. Meteorol. Mag., 47, 295–308, 1998.

Duan, L., Xiu, G., Feng, L., Cheng, N., and Wang, C.: The mercury species and their association with carbonaceous compositions, bromine and iodine in $PM_{2.5}$ in Shanghai, Chemosphere, 146, 263–271, 2016.

Fang, F., Wang, Q., and Li, J.: Atmospheric particulate mercury concentration and its dry deposition flux in Changchun City, China, Sci. Total Environ., 281, 229–236, 2001.

Fang, F., Wang, Q., and Li, J.: Urban environmental mercury in Changchun, a metropolitan city in Northeastern China: source, cycle, and fate, Sci. Total Environ., 330, 159–170, 2004.

Fang, G.-C., Wu, Y.-S., and Chang, T.-H.: Comparison of atmospheric mercury (Hg) among Korea, Japan, China and Taiwan during 2000–2008, J. Hazard. Mater., 162, 607–615, 2009.

Feng, X., Shang, L., Wang, S., Tang, S., and Zheng, W.: Temporal variation of total gaseous mercury in the air of Guiyang, China, J. Geophys. Res.-Atmos., 109, D03303, doi:10.1029/2003JD004159, 2004.

Friedli, H. R., Arellano Jr., A. F., Geng, F., Cai, C., and Pan, L.: Measurements of atmospheric mercury in Shanghai during September 2009, Atmos. Chem. Phys., 11, 3781–3788, doi:10.5194/acp-11-3781-2011, 2011.

Fu, X., Feng, X., Zhu, W., Wang, S., and Lu, J.: Total gaseous mercury concentrations in ambient air in the eastern slope of Mt. Gongga, South-Eastern fringe of the Tibetan plateau, China, Atmos. Environ., 42, 970–979, 2008a.

Fu, X., Feng, X., Zhu, W., Zheng, W., Wang, S., and Lu, J. Y.: Total particulate and reactive gaseous mercury in ambient air on the eastern slope of the Mt. Gongga area, China, Appl. Geochem., 23, 408–418, 2008b.

Fu, X. W., Feng, X., Dong, Z. Q., Yin, R. S., Wang, J. X., Yang, Z. R., and Zhang, H.: Atmospheric gaseous elemental mercury (GEM) concentrations and mercury depositions at a high-altitude mountain peak in south China, Atmos. Chem. Phys., 10, 2425–2437, doi:10.5194/acp-10-2425-2010, 2010.

Fu, X., Feng, X., Qiu, G., Shang, L., and Zhang, H.: Speciated atmospheric mercury and its potential source in Guiyang, China, Atmos. Environ., 45, 4205–4212, 2011.

Fu, X. W., Feng, X., Liang, P., Deliger, Zhang, H., Ji, J., and Liu, P.: Temporal trend and sources of speciated atmospheric mercury at Waliguan GAW station, Northwestern China, Atmos. Chem. Phys., 12, 1951–1964, doi:10.5194/acp-12-1951-2012, 2012.

Goodsite, M. E., Plane, J., and Skov, H.: A theoretical study of the oxidation of Hg^0 to $HgBr_2$ in the troposphere, Environ. Sci. Technol., 38, 1772–1776, 2004.

Gustin, M. and Jaffe, D.: Reducing the uncertainty in measurement and understanding of mercury in the atmosphere, Environ. Sci. Technol., 44, 2222–2227, 2010.

Gustin, M. S., Huang, J., Miller, M. B., Peterson, C., Jaffe, D. A., Ambrose, J., Finley, B. D., Lyman, S. N., Call, K., and Talbot, R.: Do we understand what the mercury speciation instruments are actually measuring? Results of RAMIX, Environ. Sci. Technol., 47, 7295–7306, 2013.

Gustin, M. S., Amos, H. M., Huang, J., Miller, M. B., and Heidecorn, K.: Measuring and modeling mercury in the atmosphere: a critical review, Atmos. Chem. Phys., 15, 5697–5713, doi:10.5194/acp-15-5697-2015, 2015.

Hall, B.: The gas phase oxidation of elemental mercury by ozone, in: Mercury as a Global Pollutant, Springer, 301–315, 1995.

Herndon, S. C., Onasch, T. B., Wood, E. C., Kroll, J. H., Canagaratna, M. R., Jayne, J. T., Zavala, M. A., Knighton, W. B., Mazzoleni, C., and Dubey, M. K.: Correlation of secondary organic aerosol with odd oxygen in Mexico City, Geophys. Res. Lett., 35, L15804, doi:10.1029/2008GL034058, 2008.

Holmes, C. D., Jacob, D. J., Corbitt, E. S., Mao, J., Yang, X., Talbot, R., and Slemr, F.: Global atmospheric model for mercury including oxidation by bromine atoms, Atmos. Chem. Phys., 10, 12037–12057, doi:10.5194/acp-10-12037-2010, 2010.

Hu, Q. H., Kang, H., Li, Z., Wang, Y. S., Ye, P. P., Zhang, L. L., Yu, J., Yu, X. W., Sun, C., and Xie, Z. Q.: Characterization of atmospheric mercury at a suburban site of central China from wintertime to springtime, Atmospheric Pollution Research, 5, 769–778, 2014.

Huang, J., Miller, M. B., Weiss-Penzias, P., and Gustin, M. S.: Comparison of gaseous oxidized Hg measured by KCl-coated denuders, and nylon and cation exchange membranes, Environ. Sci. Technol., 47, 7307–7316, 2013.

Jaffe, D., Prestbo, E., Swartzendruber, P., Weiss-Penzias, P., Kato, S., Takami, A., Hatakeyama, S., and Kajii, Y.: Export of atmospheric mercury from Asia, Atmospheric Environment, 39, 3029-3038, 2005.

Kim, S.-H., Han, Y.-J., Holsen, T. M., and Yi, S.-M.: Characteristics of atmospheric speciated mercury concentrations (TGM, Hg(II) and Hg(p)) in Seoul, Korea, Atmos. Environ., 43, 3267–3274, 2009.

Kleffmann, J., Gavriloaiei, T., Hofzumahaus, A., Holland, F., Koppmann, R., Rupp, L., Schlosser, E., Siese, M., and Wahner, A.: Daytime formation of nitrous acid: A major source of OH radicals in a forest, Geophys. Res. Lett., 32, L05818, doi:10.1029/2005GL022524, 2005.

Landis, M. S., Stevens, R. K., Schaedlich, F., and Prestbo, E. M.: Development and characterization of an annular denuder methodology for the measurement of divalent inorganic reactive gaseous mercury in ambient air, Environ. Sci. Technol., 36, 3000–3009, 2002.

Li, J., Sommar, J., Wängberg, I., Lindqvist, O., and Wei, S.-Q.: Short-time variation of mercury speciation in the urban of Göteborg during GÖTE-2005, Atmos. Environ., 42, 8382–8388, 2008.

Lindberg, S., Bullock, R., Ebinghaus, R., Engstrom, D., Feng, X., Fitzgerald, W., Pirrone, N., Prestbo, E., and Seigneur, C.: A synthesis of progress and uncertainties in attributing the sources of mercury in deposition, AMBIO, 36, 19–33, 2007.

Lindqvist, O. and Rodhe, H.: Atmospheric mercury-a review*, Tellus B, 37, 136–159, 1985.

Liu, B., Keeler, G. J., Dvonch, J. T., Barres, J. A., Lynam, M. M., Marsik, F. J., and Morgan, J. T.: Urban-rural differences in atmospheric mercury speciation, Atmos. Environ., 44, 2013–2023, 2010.

Lyman, S. N. and Jaffe, D. A.: Formation and fate of oxidized mercury in the upper troposphere and lower stratosphere, Nat. Geosci., 5, 114–117, 2012.

Mao, M., Jiang, W., Wu, X., Qi, F., Yuan, R., Fang, H., Liu, D., and Zhou, J.: LIDAR exploring of the UBL in downtown of the Nanjing City, Acta Scientiae Circumstantiae, 26, 1723–1728, 2006.

Marumoto, K., Hayashi, M., and Takami, A.: Atmospheric mercury concentrations at two sites in the Kyushu Islands, Japan, and evidence of long-range transport from East Asia, Atmos. Environ., 117, 147–155, 2015.

Murphy, D., Hudson, P., Thomson, D., Sheridan, P., and Wilson, J.: Observations of mercury-containing aerosols, Environ. Sci. Technol., 40, 3163–3167, 2006.

Pacyna, E. G., Pacyna, J. M., Steenhuisen, F., and Wilson, S.: Global anthropogenic mercury emission inventory for 2000, Atmos. Environ., 40, 4048–4063, 2006.

Pacyna, E. G., Pacyna, J., Sundseth, K., Munthe, J., Kindbom, K., Wilson, S., Steenhuisen, F., and Maxson, P.: Global emission of mercury to the atmosphere from anthropogenic sources in 2005 and projections to 2020, Atmos. Environ., 44, 2487–2499, 2010.

Peterson, C., Alishahi, M., and Gustin, M. S.: Testing the use of passive sampling systems for understanding air mercury concentrations and dry deposition across Florida, USA, Sci. Total Environ., 424, 297–307, 2012.

Polissar, A. V., Hopke, P. K., and Harris, J. M.: Source regions for atmospheric aerosol measured at Barrow, Alaska, Environ. Sci. Technol., 35, 4214–4226, 2001.

Ren, X., Luke, W. T., Kelley, P., Cohen, M. D., Artz, R., Olson, M. L., Schmeltz, D., Goldberg, D. L., Ring, A., and Mazzuca, G. M.: Atmospheric mercury measurements at a suburban site in the Mid-Atlantic United States: Inter-annual, seasonal and diurnal variations and source-receptor relationships, Atmos. Environ., 146, 141–152, doi:10.1016/j.atmosenv.2016.08.028, 2016.

Schroeder, W. H. and Munthe, J.: Atmospheric mercury-an overview, Atmos. Environ., 32, 809–822, 1998.

Shah, V., Jaeglé, L., Gratz, L. E., Ambrose, J. L., Jaffe, D. A., Selin, N. E., Song, S., Campos, T. L., Flocke, F. M., Reeves, M., Stechman, D., Stell, M., Festa, J., Stutz, J., Weinheimer, A. J., Knapp, D. J., Montzka, D. D., Tyndall, G. S., Apel, E. C., Hornbrook, R. S., Hills, A. J., Riemer, D. D., Blake, N. J., Cantrell, C. A., and Mauldin III, R. L.: Origin of oxidized mercury in the summertime free troposphere over the southeastern US, Atmos. Chem. Phys., 16, 1511–1530, doi:10.5194/acp-16-1511-2016, 2016.

Sommar, J., Gårdfeldt, K., Strömberg, D., and Feng, X.: A kinetic study of the gas-phase reaction between the hydroxyl radical and atomic mercury, Atmos. Environ., 35, 3049–3054, 2001.

Streets, D. G., Hao, J., Wu, Y., Jiang, J., Chan, M., Tian, H., and Feng, X.: Anthropogenic mercury emissions in China, Atmos. Environ., 39, 7789–7806, 2005.

Sun, Z., Mu, Y., Liu, Y., and Shao, L.: A comparison study on airborne particles during haze days and non-haze days in Beijing, Sci. Total Environ., 456, 1–8, 2013.

Timonen, H., Ambrose, J. L., and Jaffe, D. A.: Oxidation of elemental Hg in anthropogenic and marine airmasses, Atmos. Chem. Phys., 13, 2827–2836, doi:10.5194/acp-13-2827-2013, 2013.

Wan, Q., Feng, X., Lu, J., Zheng, W., Song, X., Han, S., and Xu, H.: Atmospheric mercury in Changbai Mountain area, northeastern China I. The seasonal distribution pattern of total gaseous mercury and its potential sources, Environ. Res., 109, 201–206, 2009a.

Wan, Q., Feng, X., Lu, J., Zheng, W., Song, X., Li, P., Han, S., and Xu, H.: Atmospheric mercury in Changbai Mountain area, northeastern China II. The distribution of reactive gaseous mercury and particulate mercury and mercury deposition fluxes, Environ. Res., 109, 721–727, 2009b.

Wang, F., Saiz-Lopez, A., Mahajan, A. S., Gómez Martín, J. C., Armstrong, D., Lemes, M., Hay, T., and Prados-Roman, C.: Enhanced production of oxidised mercury over the tropical Pacific Ocean: a key missing oxidation pathway, Atmos. Chem. Phys., 14, 1323–1335, doi:10.5194/acp-14-1323-2014, 2014.

Wang, L., Zhang, Q., Hao, J., and He, K.: Anthropogenic CO emission inventory of Mainland China, Acta Scientiae Circumstantiae, 25, 1580–1585, 2005.

Wang, Y., Zhang, X., and Draxler, R. R.: TrajStat: GIS-based software that uses various trajectory statistical analysis methods to identify potential sources from long-term air pollution measurement data, Environ. Model. Softw., 24, 938–939, 2009.

Weigelt, A., Temme, C., Bieber, E., Schwerin, A., Schuetze, M., Ebinghaus, R., and Kock, H. H.: Measurements of atmospheric mercury species at a German rural background site from 2009 to 2011–methods and results, Environ. Chem., 10, 102–110, 2013.

Weiss-Penzias, P., Jaffe, D. A., Swartzendruber, P., Dennison, J. B., Chand, D., Hafner, W., and Prestbo, E.: Observations of Asian air pollution in the free troposphere at Mount Bachelor Observatory during the spring of 2004, J. Geophys. Res.-Atmos., 111, D10304, doi:10.1029/2005JD006522, 2006.

Weiss-Penzias, P., Jaffe, D., Swartzendruber, P., Hafner, W., Chand, D., and Prestbo, E.: Quantifying Asian and biomass burning sources of mercury using the Hg / CO ratio in pollution plumes observed at the Mount Bachelor Observatory, Atmos. Environ., 41, 4366–4379, 2007.

Wood, E. C., Canagaratna, M. R., Herndon, S. C., Onasch, T. B., Kolb, C. E., Worsnop, D. R., Kroll, J. H., Knighton, W. B., Seila, R., Zavala, M., Molina, L. T., DeCarlo, P. F., Jimenez, J. L., Weinheimer, A. J., Knapp, D. J., Jobson, B. T., Stutz, J., Kuster, W. C., and Williams, E. J.: Investigation of the correlation between odd oxygen and secondary organic aerosol in Mexico City and Houston, Atmos. Chem. Phys., 10, 8947–8968, doi:10.5194/acp-10-8947-2010, 2010.

Wu, Y., Wang, S., Streets, D. G., Hao, J., Chan, M., and Jiang, J.: Trends in anthropogenic mercury emissions in China from 1995 to 2003, Environ. Sci. Technol., 40, 5312–5318, 2006.

Xu, X. and Akhtar, U. S.: Identification of potential regional sources of atmospheric total gaseous mercury in Windsor, Ontario, Canada using hybrid receptor modeling, Atmos. Chem. Phys., 10, 7073–7083, doi:10.5194/acp-10-7073-2010, 2010.

Yuan, S., Xin, Y., and Zhou, J.: Lidar Observations of the Lower Atmosphere in Hefei, Chinese J. Atmos. Sci., 29, 387–395, 2005.

Zhang, H., Fu, X. W., Lin, C.-J., Wang, X., and Feng, X. B.: Observation and analysis of speciated atmospheric mercury in Shangri-La, Tibetan Plateau, China, Atmos. Chem. Phys., 15, 653–665, doi:10.5194/acp-15-653-2015, 2015.

Zhang, L., Wang, S. X., Wang, L., and Hao, J. M.: Atmospheric mercury concentration and chemical speciation at a rural site in Beijing, China: implications of mercury emission sources, Atmos. Chem. Phys., 13, 10505–10516, doi:10.5194/acp-13-10505-2013, 2013.

Zhang, L., Wang, S., Wang, L., Wu, Y., Duan, L., Wu, Q., Wang, F., Yang, M., Yang, H., and Hao, J.: Updated Emission Inventories for Speciated Atmospheric Mercury from Anthropogenic Sources in China, Environ. Sci. Technol., 49, 3185–3194, 2015.

Zhu, J., Wang, T., Talbot, R., Mao, H., Hall, C. B., Yang, X., Fu, C., Zhuang, B., Li, S., Han, Y., and Huang, X.: Characteristics of atmospheric Total Gaseous Mercury (TGM) observed in urban Nanjing, China, Atmos. Chem. Phys., 12, 12103–12118, doi:10.5194/acp-12-12103-2012, 2012.